Merging flexibility with superinsulation: machinable, nanofibrous pullulan-silica aerogel composites

Shanyu Zhao [1*], Olivier Emery [1], Anja Wohlhauser [2], Matthias M. Koebel [1], Christian Adlhart [2], Wim J. Malfait [1*]

[1] *Laboratory for Building Energy Materials and Components, Empa, Überlandstrasse 129, 8600 Dübendorf, Switzerland*

[2] *Institute of Chemistry and Biotechnology, Zurich University of Applied Sciences ZHAW, Einsiedlerstrasse 31, CH-8820 Wädenswil, Switzerland*

* Corresponding authors: shanyu.zhao@empa.ch, wim.malfait@empa.ch

Abstract: Freeze-dried nanofibrous scaffolds are flexible, but typically have high thermal conductivities. Conversely, silica aerogel has an ultra-low thermal conductivity, but is brittle. Here, the impregnation of pullulan/PVA nanofiber scaffolds with hydrophobic silica aerogel decreased the thermal conductivity from 31.4 to 17.7 mW/(m·K). The compatibility between the silylated nanofibers and the silica aerogel promotes the overgrowth of silica particles onto the fiber surfaces and the fiber incorporation. The composites display improved compressive and tensile properties compared to the neat pullulan scaffold and silica aerogel. The composite's E-modulus is 234 kPa compared to 4 kPa for the pullulan scaffold and 102 kPa for the silica aerogel. The composite's tensile strength is five times higher than that of the silica aerogel. Because of its reduced brittleness, the pullulan-silica aerogel composites can be shaped using a sharp blade. The composites can sustain uniaxial compression up to 80%

strain, but the decompressed composites display two times higher densities because the strain is partially irreversible. This densification reduces thermal conductivity to 16.3 mW/(m·K) and increases final compressive strength by a factor of seven. Both the as prepared and densified composites demonstrate unique material properties in terms of thermal conductivity, mechanical strength and machinability.

Keywords: nanocomposite; polysaccharide; nanofibers; hybrid aerogels; densification

1. Introduction

Biopolymer aerogels were among the first aerogels ever synthesized [1] and have seen a strong revival in the last decade, motivated by the potential for new technical applications of aerogels, the search for more sustainable aerogel precursors, and a strong motivation from the academic community to add value to biopolymer materials [2]. Among biopolymers, polysaccharides have received particular attention, because they are available in large quantities from agricultural production, often as a by-product (pectin) or waste material (cellulose, chitin), and their use as a feedstock for advanced materials could be a great value proposition. Many biopolymer aerogel studies target applications in thermal insulation [3-7], the most prominent industrial application of silica aerogel, but the vast majority of materials produced do not reach the ultra-low thermal conductivities associated with silica aerogels [2, 8], despite some notable exceptions with thermal conductivities below 20 mW/(m·K), for example from pectin [3, 9], chitosan [10, 11] and cellulose [8, 12-14]. In addition, concerns about long-term stability have not yet been fully addressed.

Cellulose, alginate, pectin, starch carrageenan and chitin/chitosan account for the vast majority of polysaccharide aerogel studies [2, 15-17], but alternative polysaccharides have received far less attention in aerogel research. Pullulan is a starch-derived polysaccharide based on maltotriose units connected by α-1,6 glycosidic bonds. Recently, low-density, freeze-dried scaffolds have been prepared from electrospun pullulan-polyvinyl alcohol nanofibers [18-21]. These novel materials have a strong application potential in wound healing, gas filtration and oil-water separation, but do not possess a sufficiently high fraction of mesopores to qualify as thermal superinsulators, which is confirmed by the thermal conductivity measurements presented in this work (see below).

Here, we impregnated nanofibrous, silylated pullulan scaffolds [18] with silica aerogel through a sol impregnation based process. The rationale is that the small pore sizes in silica aerogels, which are below the mean free path length of air (~70 nm at 1 bar and 25°C), will reduce the gas phase thermal conduction. At the same time, the tortuosity of the silica and pullulan nanofiber networks should limit the solid phase conduction. Recent publications on aerogel materials and composites have combined silica aerogel with (bio)polymers and fibers over a wide range of length scales. The industrially most relevant approach is the impregnation of silica aerogel into macroscopic fiber blankets [22-25]. The use of nanofibers represents an intermediate length scale, where either the nanofibers are added to the silica sol in a cogelation approach [26-34]or a preformed nanofibrous scaffold is impregnated with a silica sol [35-37]. The latter approach is the one pursued in this study. At the smallest length scale, the (bio)polymers or their monomeric precursors have been incorporated as individual molecules, first through post-modification [38-40] and more recently through co-gelation approaches [41-46]. Finally, biopolymer-free, silicone-like rather than silica-like aerogels with excellent thermal and mechanical properties have been prepared from functionalized silanes [47, 48].

Here, we aim to synthesize a material that combines the excellent thermal conductivity of silica aerogel with the flexibility of nanofibrous pullulan scaffolds. Therefore, previously fabricated, silylated nanofibrous pullulan scaffolds were impregnated with a silica sol, followed by gelation, aging, hydrophobization and supercritical drying. The resulting nanocomposites were then analysed in terms of their thermal and mechanical properties.

2. Experimental

2.1 Synthesis

The preparation and characterization of the pullulan/PVA nanofibrous scaffolds is detailed in a previous publication [18] and will only be summarized here. Pullulan/PVA nanofibers were prepared by free liquid surface electrospinning an aqueous solution of 4 wt% pullulan and 6 wt% polyvinylalcohol (PVA) at 80 kV. The recovered nanofibrous membrane was cut into ca. 1 cm^2 pieces and dispersed in 1,4-dioxane for 20 minutes at 13000 rpm. The homogenous dispersion was cast into a mold, frozen, freeze-dried for 48 h and thermally cross-linked at 180°C for 40 minutes. Finally, the cross-linked pullulan/PVA scaffolds were hydrophobized for 24 h by chemical vapour deposition in a desiccator saturated in trichloro(octyl)silane, followed by the elimination of excess silane and HCl under vacuum (10 mbar, 2h).

The pullulan-silica aerogel composites were prepared according to Figure 1. A polyethoxydisiloxane (PEDS) sol stock solution, i.e. pre-polymerized tetraethoxysilane (TEOS) with a water-to-TEOS molar ratio of 1.5 and a SiO_2 equivalent concentration of 20 wt% in ethanol, was used as silica precursor. 30 ml of PEDS solution was diluted with 120 ml ethanol (F25-A-MEK, 94 wt% ethanol denatured with 2% methyl ethyl ketone, Alcosuisse, Switzerland) to a silica concentration of 4 wt%. Then, 5 ml of water and 1.2 ml of 5.5 M NH_4OH aqueous solation were added to trigger gelation. The activated sol was portioned into 6 aliquots of 20 ml and cast into a prefabricated pullulan/PVA nanofibrous scaffolds, followed by 5 minutes degassing in a vacuum chamber (~10 mbar) to remove air bubbles trapped in the fiber scaffold. Gelation typically occurred 10 to 15 minutes after the base addition at room temperature. The gelled composites were covered with ethanol and aged overnight at 55°C. The aged gels (120 ml in total) were hydrophobized by immersing them in a mixture of hexamethyldisiloxane (240 ml), ethanol (8.82 ml) and 37% HCl (0.96 ml). After washing with ethanol once, the gels were dried supercritically in a SCF extractor (Autoclave 4334/A21-1, Separex, France). A set of reference silica aerogels was also prepared according to the same procedure, but without the nanofibrous pullulan scaffold. The surfaces of the

dried samples were polished prior to performing the mechanical tests and thermal conductivity measurements, with 400 grit sandpaper to remove the edges (menisci), and 2000 grit paper for finishing.

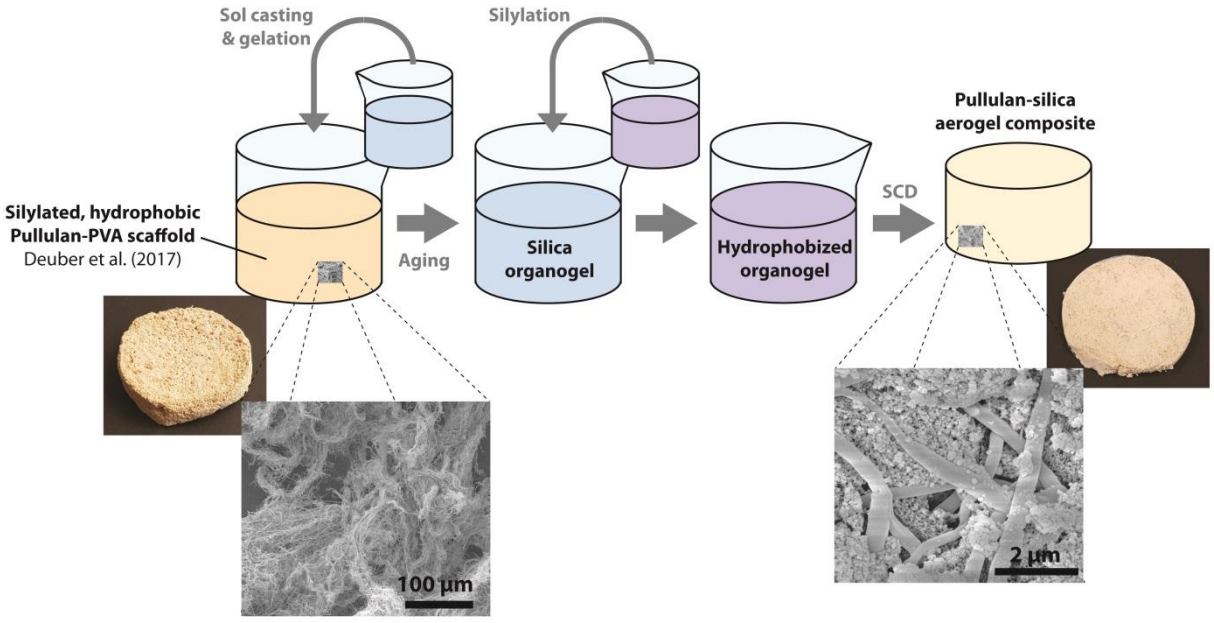

Figure 1. Synthesis scheme for the pullulan/PVA-silica aerogel nanocomposites.

2.2 Characterization

Density and Brunauer-Emmett-Teller (BET). The bulk density was calculated from the mass and volume of the regularly shaped, cylindrical samples and the skeletal density was approximated by the linear combination of the known skeletal densities of the constituents: silica aerogel 2.0 g cm^{-3}, pullulan 1.5 g cm^{-3}, and PVA 1.2 g cm^{-3}. The BET specific surface of the composites was determined by nitrogen sorption after degassing at 100°C and 133 mbar for 20 h. Nitrogen adsorption and desorption isotherms were obtained at liquid nitrogen temperature on a Micromeritics TriFlex instrument with 15 seconds equilibration time. The specific surface area of the samples was determined by the Brunauer–Emmett–Teller (BET) method. The pore size distributions and pore diameter D'_{pore} were obtained from the

desorption branch of the isotherm using the Barrett–Joyner–Halender (BJH) model, despite the known limitations of nitrogen sorption analysis in determining pore volume and pore size [49].

SEM characterization and Energy Dispersive X-ray (EDX). Composite aerogels were analyzed after coating with a platinum layer of nominally 10 nm, which refers to the thickness of the Pt coating on the quartz sensor, whereas the actual thickness on the sample may be quite a bit thinner because of the high surface area of the samples. SEM analysis of all materials was performed on a FEI Nova NanoSEM 230 instrument (FEI, Hillsboro, Oregon, USA) at an accelerating voltage of 10 kV and a working distance of 5 mm. The elemental composition was obtained by using energy dispersive X-ray spectrometry (EDX, INCA X-Act, Oxford Instruments, UK) using 20 kV acceleration voltage and a 6mm working distance.

Solid-state NMR spectra were collected on a Bruker Avance III spectrometer equipped with a wide-bore 9.4 T magnet with ^{1}H, ^{13}C and ^{29}Si Larmor frequencies of 400.2, 100.6 and 79.5 MHz, respectively. ^{1}H-^{13}C cross polarization (CP) and ^{1}H-^{13}C CP spectra were collected with respective contact times of 2 and 5 ms, 7 mm zirconia rotors, a magic angle spinning (MAS) rate of 4 kHz, a recycle delay of 2 s and between 180 and 27000 scans, depending on the sample.

Mechanical properties

Uniaxial compression tests of the composites were performed on monolithic cylindrical samples (~22 mm diameter, ~ 30 mm high) using a universal materials testing machine (Zwick/Z010, Zwick/Roell, Germany), equipped with a 10 kN force transducer (KAP-S, AST Gruppe GmbH, Germany) in a controlled environment (23^{o}C, 50% relative humidity). Elastic moduli were measured in compression mode and were calculated from the linear region of the stress-strain curves which typically occurred at 3 ± 2 % strain. A constant deformation rate of 1 mm/min was used and compressive strength values were taken at the first noticeable sign of cracking. Tensile strength was estimated by the Brazilian split test, which is typically used in

cements and ceramic materials and entails the compression of a cylindrical sample lying on its side [50]. The tensile strength σ_T can be calculated from the geometry and the compressive force F as shown in Eq. 1, where D and L are the diameter and length of the samples. The test setup was the same apparatus as used for the uniaxial compression test, but the loading cell was adapted with a customized holder to fit to the cylindrical samples.

$$\sigma = \frac{F}{\pi\left(\frac{D}{2}\right)L} \quad (1)$$

Thermal conductivity

Thermal conductivity measurements of flat cylindrical tiles of approximately 45 mm in diameter and 7 mm thickness were carried out on a custom-built guarded hot plate device designed for small samples / low thermal conductivity materials (guarded zone: 50×50 mm^2, measuring zone: 25×25 mm^2) at a temperature of 25°C on the hot side and 10°C on the cold side (the apparatus is shown in Figure S1, SI).[51] In order to be consistent with measurements according to the European standards [52], calibration measurements were carried out using conventional expanded polystyrene samples measured first in the standard test equipment (conventional guarded hot-plate device) and then cut into smaller pieces to be measured in a second run in the smaller apparatus. The accuracy of the custom-built device was determined to be ±1.0 mW/(m·K) by measuring over 20 samples with known thermal conductivities in the range of 15 to 25 mW/(m·K).

Water contact angle

The surface wettability of samples was evaluated by water contact angle measurement using a Contact Angle System OCA (Dataphysics TBU 90E, Germany), combined with a high-speed camera. Water droplets were deposited directly on the top or bottom surfaces of the samples. Two measurements were performed per sample and averaged. The volume of the water droplet was 5 µL, and the tip used was a precision stainless steel tip (Gauge 32, EFD).

3. Results and Discussion

3.1 Chemistry, microstructure and the pullulan-silica aerogel interface

The ^{1}H-^{29}Si CP MAS NMR spectrum of the pullulan/PVA scaffolds (Figure 2a) displays no observable signals, indicating that the concentration of grafted octylsilyl groups is too low to be detected by our current solid-state NMR experiment. This is not surprising, given the relatively low surface area (~10 m^2/g predicted from a nanofiber diameter of 240±55 nm) and resulting low concentration of octylsilyl groups from the chemical vapour deposition of trichloro(octyl)silane, with <5 wt% weight gain or <1 wt% of Si [18]. The grafted silanes however can be detected as a (weak) Si signal in the EDX spectra of the silylated pullulan/PVA sponges (Figure S1). The ^{1}H-^{29}Si CP MAS NMR spectrum of both the reference silica aerogel and the pullulan-silica aerogel nanocomposites displays the typical peaks from the trimethylsilyl (TMS) groups and the Q^n species of the silica aerogel, where Q^n is a Si atom coordinated by n bridging oxygens (≡Si-O-Si≡) and 4-n non-bridging oxygens (≡Si-OH or ≡Si-OCH_2CH_3).

The ^{1}H-^{13}C CP MAS NMR spectrum of the pullulan/PVA scaffold displays the bands expected for a mixture of pullulan [53] and PVA [54]. In addition, bands related to the caramelization products that originate from the thermal cross-linking step are present [55]. Note that, as for the ^{1}H-^{29}Si CP spectrum, the signal from the grafted octylsilyl groups is not intense enough to be detected in the ^{1}H-^{13}C CP spectrum. The ^{1}H-^{13}C CP MAS NMR spectrum of the reference silica aerogel displays three main bands, related to trimethylsilyl groups and the methyl and methylene groups of the ethoxy groups (≡Si-OCH_2CH_3), as expected for a PEDS derived silica aerogel prepared in an ethanol-based solvent [56, 57]. The ^{1}H-^{13}C CP MAS NMR spectrum of the pullulan-silica aerogel nanocomposite closely

205 resembles a linear combination of the spectra of the neat pullulan/PVA sponge (~25% of
206 signal) and that of the reference silica aerogel (~75% of signal), in proportions that are
207 consistent with the densities of the pullulan/PVA scaffold (0.030 g/cm^3), reference silica
208 aerogel (0.071 g/cm^3) and pullulan-silica aerogel nanocomposite (0.099 g/cm^3).
209
210 Although CP NMR spectra are not quantitative in nature, a comparison of the relative peak
211 intensities for different samples does provide a qualitative measure of species concentrations
212 because the CP conditions were kept constant between the different measurements. The
213 TMS/Q^n peak intensity ratio is higher in the ^{1}H-^{29}Si spectrum of the reference silica aerogel
214 than for the pullulan-silica aerogel composite (Figure 2a), indicating that the former is more
215 completely hydrophobized. A higher degree of hydrophobization should be associated with a
216 higher degree of polymerization because oxygen bridges (≡Si-O-Si$(CH_3)_3$) are formed during
217 the grafting reaction of TMS, and this is confirmed by the higher Q^4/Q^3 peak ratio for the
218 reference silica aerogel. Finally, the higher hydrophobization degree for the reference silica
219 aerogel is also confirmed by the higher TMS/ethoxy peak ratios in the ^{1}H-^{13}C spectrum
220 (Figure 2b). In previous studies on silica-pectin and silica-chitosan hybrid aerogels, prepared
221 from molecular rather than nanofibrous polysaccharides, we have observed a similar effect,
222 i.e. a less complete hydrophobization for the hybrid aerogels compared to neat silica aerogel
223 [42, 43]. Note that this difference in TMS concentration does not affect the water contact
224 angle, which is the same for both the reference silica aerogel and the composite (~140°, Table
225 1).
226

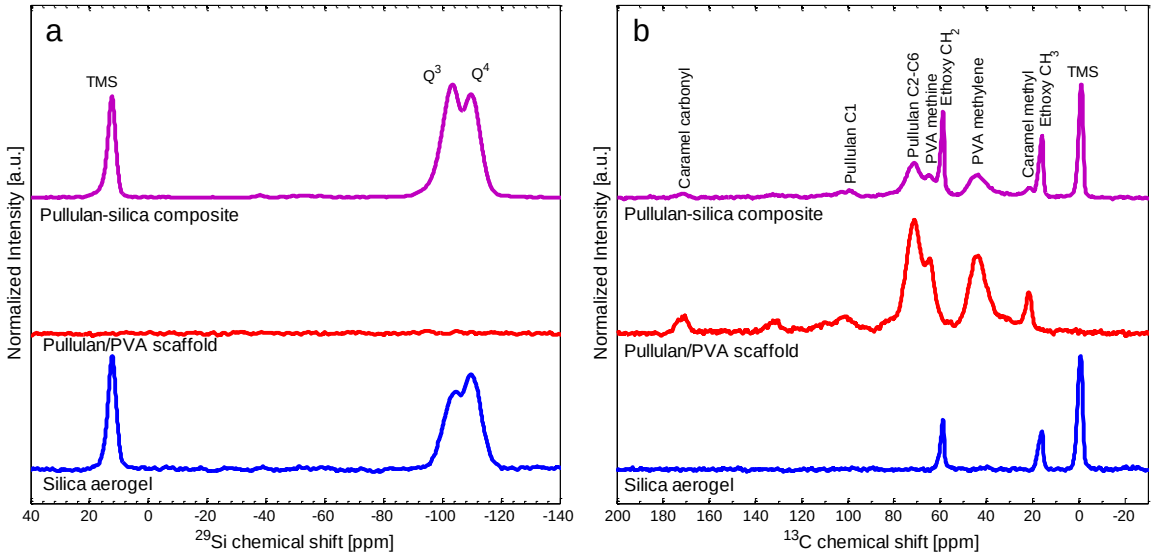

Figure 2. Solid-state MAS NMR spectra of the reference silica aerogel, silylated pullulan/PVA scaffold, and pullulan-silica aerogel composite; a) ^{1}H-^{13}C CP spectra; b) ^{1}H-^{29}Si CP spectra.

The pullulan/PVA scaffolds display a hierarchical pore structure with major cellular pores from the freeze-drying process, separated by pore walls with high local concentrations of entangled nanofibers with minor pores in between. The pullulan/PVA nanofibers themselves have fiber diameters on the order of 250 nm, consistent with those prepared in an earlier study [18], and have smooth surfaces. Locally, nanoparticle aggregates formed on the pullulan/PVA nanofibers (Figure 3b) and EDX analysis (Figure S1) confirms these to be rich in Si. These aggregates are clearly originating from the trichloro(octyl)silane chemical vapour deposition process. The Si content of the smooth fiber surfaces, further away from the nanoparticle aggregates, is close to the EDX detection limit, i.e. either just below or just above the detection limit, depending on the location of the analysis (Figure S1).

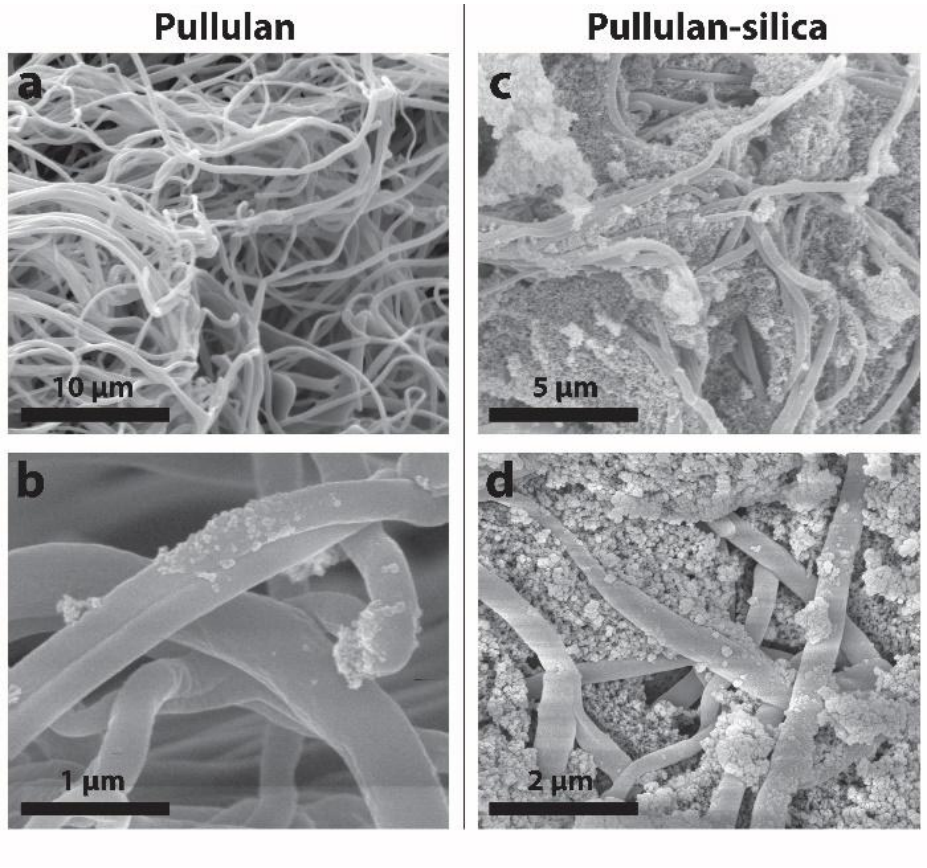

Figure 3. SEM images of a silylated pullulan/PVA scaffold (a,b) and the pullulan-silica aerogel composites (c,d).

The SEM images of the pullulan-silica aerogel nanocomposites confirm that the silica aerogel phase completely fills the interstitial pores between the pullulan/PVA nanofibers and no macroscopic voids are present in the composites (Figure 3c,d). The silica aerogel phase itself displays the particle-network mesostructure typical for silica aerogels, with secondary particles of around 20 to 50 nm in diameter (Figures 4, 3d). The mesoporosity of the silica aerogel inside the pullulan-silica aerogel nanocomposites is confirmed by nitrogen sorption analysis (Figure S2), with a strong signal in the capillary condensation regime, a specific surface area (S_{BET}) of 617 m^2/g and a BJH mesopore volume of 2.4 cm^3/g. Note that the specific surface area and specific BJH mesopore volume of the silica aerogel phase within the composite is most likely higher than the values reported above, because approximately 30%

of the mass of the composite consists of low surface area pullulan/PVA fibers. The average pore diameter, as approximated from the density and surface area, assuming cylindrical pores, shown in Equation 1.

$$D'_{pore} = 4\,V_{pore}/S_{BE} \quad (1)$$

where $V_{pore} = 1/\rho_{envelope} - 1/\rho_{skeletal}$, is around 60 nm.

In a recent study, we observed a strong beneficial effect of silylation on the mechanical properties of cellulose foam-silica aerogel nanocomposites [35] and the same mechanism is probably acting in the pullulan-silica aerogel system. The pullulan/PVA nanofiber surfaces in the composites are overgrown with colloidal silica secondary aerogel particles (Figure 4), suggesting a good interfacial compatibility between the silylated pullulan/PVA surface and the silicon alkoxide based silica sol. The high compatibility is mediated by the nanofiber surface modification with a trichloro(octyl)silane derived polysiloxane CVD layer that benefits from the high reactivity of the chlorosilanes to form ≡C-O-Si≡ bonds on the biopolymer surface. The silica growth on the silylated nanofibers progresses through ≡Si-O-Si≡ bond formation, which offsets the somewhat lower reactivity of the alkoxysilanes during the silica sol-gel impregnation step compared to the higher reactivity of the chlorosilanes during the chemical vapour deposition. CVD silane mediated silica overgrowth on the pullulan/PVA nanofibers (see schematic sketch in Figure 4) ensures that the nanofibers are fully incorporated into the silica aerogel structure, also mechanically, and improves the reinforcement effect that the nanofibrous scaffold has on the composite.

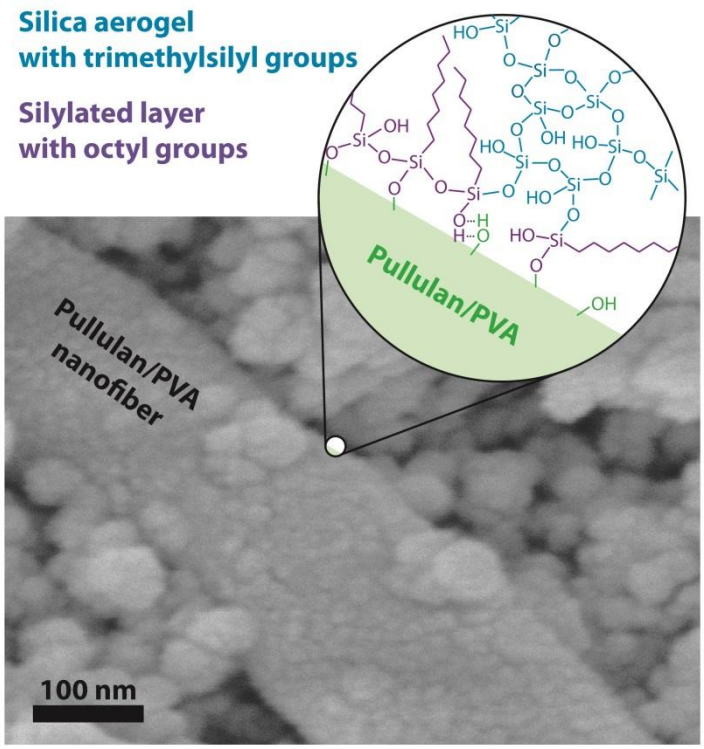

Figure 4. SEM image of a pullulan/PVA-silica aerogel composite and a schematic overview of the chemical interactions at the interface between the silylated nanofiber and the silica aerogel.

3.2 Thermal and mechanical properties

With a thermal conductivity of 31.4 mW/(m·K) (Table 1, Figure 5b), the hydrophobic, freeze-dried pullulan/PVA scaffolds are good thermal insulators in their own right, with a performance that is similar to high performance mineral wool or polystyrene insulation. However, they are not superinsulators because the pores between the pullulan/PVA nanofibers are large (between 1 to 1000 µm) compared to the mean free path length of the air molecules (~70 nm STP) and hence, gas phase conduction is not reduced by the Knudsen effect. The reference silica aerogel in this study has a thermal conductivity of 17.5 mW/(m·K), i.e. well below the ~26 mW/(m·K) typical for standing air, because the gas phase conduction within the aerogel mesopores is limited by the Knudsen effect. However, the

thermal conductivity of the reference silica aerogel is somewhat higher than that of an optimized silica aerogel because of its specifically designed density (0.071 g/cm^3) below the optimum for minimal thermal conductivity (typically near 0.120 g/cm^3 [50, 58]). With a value of 17.7 mW/(m·K), the pullulan-silica aerogel composite has a near-identical thermal conductivity to the reference silica aerogel, which indicates that the solid conduction through the pullulan-fiber network is not significant. This is not unexpected as solid conduction through low-density fiber networks is generally low [59, 60]. The ultra-low thermal conductivity of the pullulan-silica aerogel composite is comparable to that of high quality silica aerogel and places this hybrid material among the very best silica-(bio)polymer hybrid aerogels in terms of thermal conductivity [41-43, 61-63], in contrast to classical polymer-reinforced aerogels (X-aerogels) for which the, admittedly much stronger, increase in mechanical strength is accompanied by a large penalty in density and thermal conductivity [38, 64, 65].

The compression properties of the freeze-dried pullulan/PVA scaffolds have been described in detail before [18]: the materials can sustain compression stress without rupture up to at least 80%, but display a low *E* modulus and final compressive strength commensurate with their low density (Table 1, Figure 5a,b). The reference silica aerogel displays compressive properties expected for low density silica aerogels (0.071 g/cm^3): unlike the more elastic and brittle intermediate and high density silica aerogels [50], the reference aerogels studied plastically deform and can sustain uniaxial compression up to at least 80% strain. However, several minor stress release events - linked to multiple crack initiations - are evident from the stress-strain curves between 50 and 80% strain for some samples, leading to a relatively wide scatter in final compressive strength, i.e. σ_{80} (Figure 5a). The pullulan-silica aerogel composites also sustain uniaxial compression up to at least 80%, but have smoother, more reproducible stress-strain curves. The composites display an increase in E modulus by a factor

of 56 and 2.3 compared to the neat pullulan/PVA scaffolds and the reference silica aerogel, respectively, with similar increases in σ_{80}. The tensile strength of the silica aerogel and pullulan-silica aerogel composite was estimated from the Brazilian split test [50] and is nearly five times higher for the composite than for the reference silica aerogel (Table 1). As for the compression tests, the stress-strain curves of the pullulan-silica aerogel composite are smooth, whereas those of the reference silica aerogel display minor episodes of step-wise stress releases that decrease the tensile strength and lead to a large sample-to-sample variation (Figure S3). Thanks to their improved compression and tensile properties, the pullulan-silica aerogel composites can be shaped simply by cutting with a sharp blade (Figure 5c), a remarkable feature for silica aerogel composites.

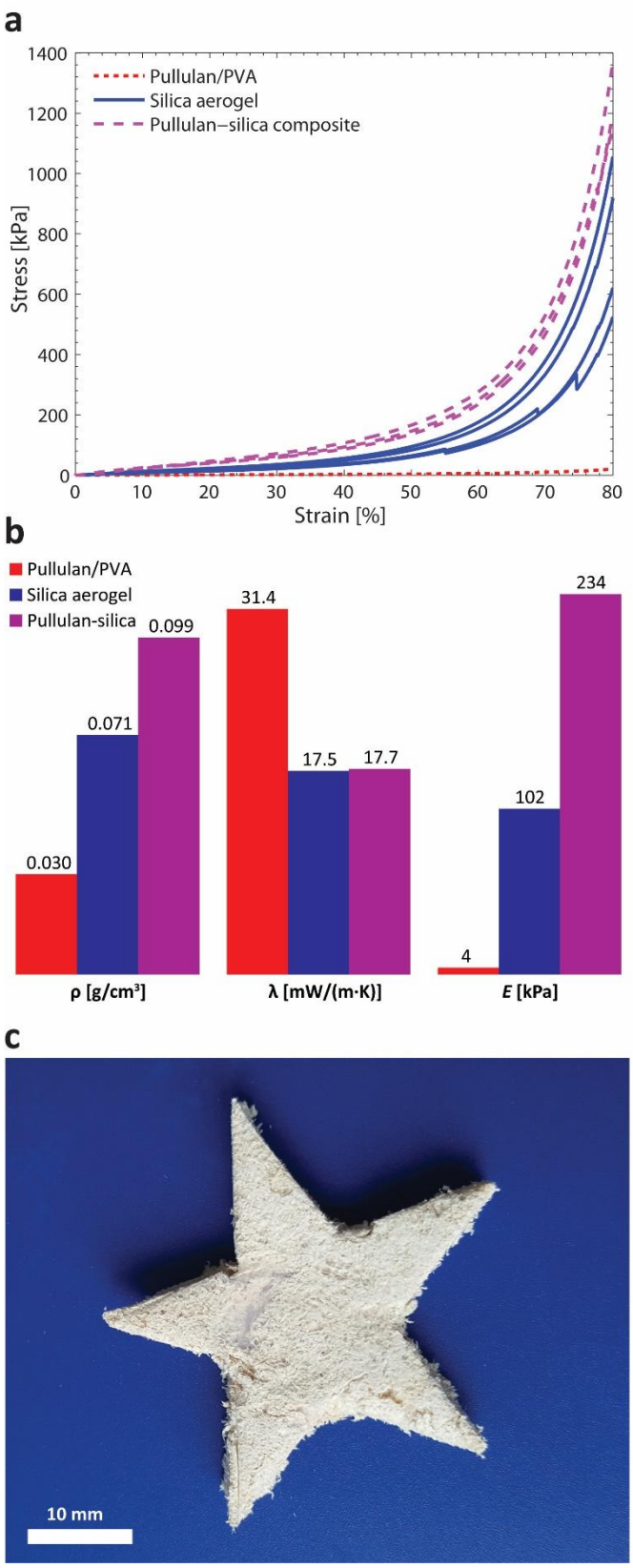

Figure 5. a) Stress-strain curves during uniaxial compression upon first compression; each curve corresponds to a different sample. b) Thermal and mechanical properties. c) Demonstration of the ability to shape the pullulan-silica aerogel composites by cutting.

Table 1. Density, thermal conductivity and mechanical properties.

						Compression (cylinders)			Compression (plates)				Brazilian test	
	ρ		λ		WCA	*E*		ε_{max}	σ_{50}		σ_{80}		σ_T	
	[g/cm^3]	±	[mW/(m·K)]	±	[°]	[kPa]	±	[%]	[kPa]	±	[kPa]	±	[kPa]	±
Pullulan/PVA scaffolds	0.030	0.004	31.4	1.7	132	4	-	>80	8	-	48	-	n.a.	
Silica aerogel	0.071	0.002	17.5	0.6	140	102	27	>80	57	15	470	84	7	8
Pullulan-silica composite	0.099	0.005	17.7	0.9	141	234	23	>80	164	30	818	105	34	7
Compressed composite	0.182	0.015	16.3	1.1	n.a.	n.a.		n.a.	1057	-	6121	-	n.a.	

n.a.: not analyzed

WCA: water contact angle

±: calculated as 1.96·STD/n$^{1/2}$, where n is the number of measurements

3.3 Improving thermal and mechanical properties through uniaxial irreversible compression

A relatively low SiO_2 equivalent concentration in the silica sol was selected for the synthesis of the reference and composite aerogels and this leads to a low density of the resulting aerogels (Table 1). This low density in turn leads to thermal conductivities that are somewhat higher than usual for silica aerogel, presumably because the low densities leads to larger pore sizes and a sub-optimal suppression of the gas phase thermal conductivity [50, 58]. Recently, Plappert et al. [12] irreversibly compressed pre-formed low-density cellulose aerogels to decrease the thermal conductivity and increase the mechanical strength. The same approach was applied here. The pullulan-silica aerogel nanocomposites can sustain uniaxial compression up to 80% strain, but display double the density after decompression, compared to the original composite (0.183 versus 0.101 g/cm^3). In other words, part of the strain is irreversible. The compressed pullulan-silica aerogel composite displays a 1.4 mW/(m·K) lower thermal conductivity of 16.3 mW/(m·K). The reduction in thermal conductivity is consistent with a decrease in gas phase conduction due to a decrease in average pore size: the compression treatment reduces the average pore size from ~60 to 35 nm, as calculated from the density, pore volume and BET surface area (560 m^2/g), to well below the mean free path of air (70 nm at STP). More strikingly, the mechanical properties are improved by nearly an

order of magnitude, for example the maximum compressive strength (σ_{80}) increased from 0.82 to 6.12 MPa (Table 1, Figure 6). The mechanical properties of the pullulan foam, silica aerogel, composite aerogel, and compressed composite aerogel follow a single power-law behaviour as a function of density, for example both σ_{80} and σ_{50} correlate with $\rho^{2.7}$ (Figure S4). Power law behaviour is common for (biopolymer) aerogels [2, 26], but it is somewhat surprising that the very different materials studied here define a single trend. This indicates that, at least for the investigated systems, density is the primary factor that determines the compressive properties, with less prominent effects from the composition of the solid phase (pullulan/PVA versus silica) or the morphology of the microstructure (nanofibrous foam versus particle based network). In summary, permanent densification through uniaxial compression provides a substantial improvement of the thermal and the mechanical properties of the composites, without compromising machinability (Figure S5).

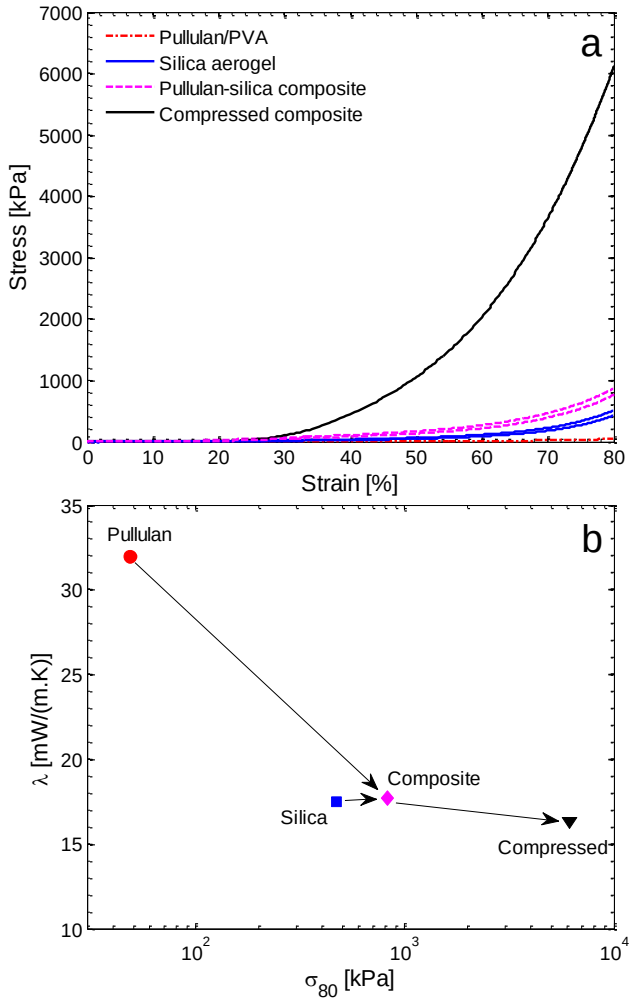

Figure 6. a) Stress-strain curves under uniaxial compression of sample plates. b) Ashby plot of thermal conductivity versus σ_{80}.

3.4 Comparison with constituent reference compounds and other hybrid aerogels

The thermal and mechanical properties illustrate that the pullulan-silica aerogel composite is more than just the sum of its parts and has superior properties compared to both the neat pullulan/PVA scaffold and the neat silica aerogel. This is true for the mechanical properties collected under lab scale conditions, e.g. compression testing on polished cylinders, but even more so for the real world behaviour, e.g. in terms of machinability, fragility and dust release. The spider plot in Figure 7a compares the four materials studied here in terms of their thermal

insulation performance, machinability, non-brittleness, dust release, hydrophobicity and E modulus. The silica aerogel phase imparts the as-prepared and densified composites with an ultra-low thermal conductivity. The pullulan/PVA scaffolds impart the composites with a low dust release and machinability. As discussed above, the *E* modulus of the composites benefits from the higher density, particularly for the densified composite, but also for the as-prepared samples (Table 1, Figures 5, 6, S4) and because of the power law dependence of the compression properties on density, these effects exceed the benefits expected for a simple additive behaviour. Importantly, no application relevant properties are worse in the composite than in the neat counterparts.

Some application relevant properties of silica aerogel hybrids from the literature are plotted in Figure 7b for comparison. Standard silica aerogel, with a density of 0.100 to 0.120 g/cm^3, displays elastic compression behaviour, but is very brittle and not machinable [50]. The closest materials in terms of microstructure and synthesis procedure are the silica aerogel – nanofibrillated cellulose foam composites we prepared in a previous study, which were also a major inspiration for the current work. In that study, silylation of the biopolymer foam was found to improve the interfacial compatibility with silica aerogels [18, 66], but because the scaffold was impregnated with a standard density silica aerogel, the mechanical reinforcement effects were rather limited: because of its relatively low density, the silica aerogel employed in the current study is non-brittle [50], and combined with the flexible, highly machinable pullulan-PVA scaffolds, the composites inherit the merits from each component and synergistically enhance the overall properties, particularly in terms of dust release and machinability. Macroscopic fiber blankets filled with silica aerogel [22, 23] are also easy to cut into shape, but typically suffer from a high dust release, in contrast to the composites presented in this study, which display a very low dust release, presumably because of the high interfacial compatibility (Figure 4) and because the nanofibrous scaffolds are more effective

at locking fractured aerogel particles in place (Figure 3). Classical polymer reinforced aerogels (X-aerogels) have excellent mechanical properties, with particularly high E-moduli [65], but strongly increased thermal conductivities. In contrast, recent (bio)polymer aerogel reinforced silica aerogels prepared by co-gelation approaches have good thermal properties, a low dust release, but poor machinability [41-43]. Finally, single phase organic-silica aerogels based on functional organosilanes have been developed with excellent thermal and mechanical properties [47, 48]. Most of the cited materials above, and also the pullulan-silica aerogel composites developed here, have not yet been evaluated for a range of other application relevant properties, including fire behaviour and long term stability, but these are beyond the scope of a scientific study.

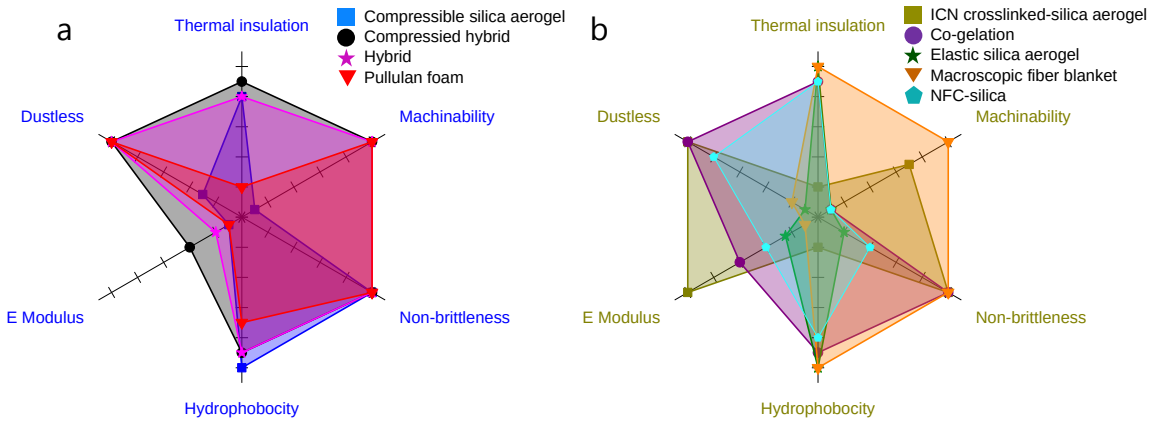

Figure 7. Comparison of thermal, mechanical and hydrophobic properties of a) the compressible silica aerogel (0.070 g/cm^3), freeze dried pullulan scaffolds, and their as-prepared and compressed hybrids developed in this study; b) PU-silica X-aerogels [65], co-gelation polymer-silica aerogel hybrids [41-43], macroscopic fiber aerogel blankets [22, 23], NFC-silica aerogel nanocomposites [35], elastic silica aerogel (0.120 g/cm^3) [50].

Conclusions

Recently, a wide variety of sol-gel derived, freeze-dried scaffolds have been prepared from (bio)polymer nanofibers. Although these materials often have a low thermal conductivity, in our case equivalent to that of high quality conventional thermal insulation, this is not low enough to offset the more complex synthesis procedure. In addition, the materials are not competitive with classical aerogels in terms of thermal conductivity. In this study, we have demonstrated that the impregnation of silica aerogel decreases the thermal conductivity of the pullulan/PVA scaffold from 31.4 to 17.7 mW/(m·K). At the same time, the pullulan-silica aerogel nanocomposites display strongly improved compression and tensile properties by a factor of 2 and 5 as compared with pure silica aerogel, which makes them easy to shape and machine. Densification of the as-prepared, low-density nanocomposites further reduces thermal conductivity to 16.3 mW/(m·K) and strongly increases the mechanical strength about an order of magnitude and densification through uniaxial compression provides a simple way to tune the thermal and mechanical properties towards specific applications.

Acknowledgements

We thank Beatrice Fischer and Daniel Rentsch for providing access to the mechanical testing and NMR instruments, respectively. The NMR spectrometer was funded in part by SNF grant 150638.

Data availability

The raw/processed data required to reproduce these findings cannot be shared at this time due to technical or time limitations.

References

[1] S.S. Kistler, Coherent Expanded Aerogels and Jellies, Nature 127 (1931) 741-741 https://doi.org/10.1038/127741a0.

[2] Z. Shanyu, M.W. J., G.A. Natalia, K.M. M., N. Gustav, Biopolymer Aerogels and Foams: Chemistry, Properties, and Applications, Angew. Chem. Int. Ed. 57(26) (2018) 7580-7608 https://doi:10.1002/anie.201709014.

[3] S. Groult, T. Budtova, Thermal conductivity/structure correlations in thermal super-insulating pectin aerogels, Carbohydr. Polym. 196 (2018) 73-81 https://doi.org/10.1016/j.carbpol.2018.05.026.

[4] H.-B. Zhao, M. Chen, H.-B. Chen, Thermally insulating and flame retardant polyaniline/pectin aerogels, ACS Sustainable Chem. Eng. 5(8) (2017) 7012-7019 DOI: 10.1021/acssuschemeng.7b01247.

[5] C. Jiménez-Saelices, B. Seantier, B. Cathala, Y. Grohens, Spray freeze-dried nanofibrillated cellulose aerogels with thermal superinsulating properties, Carbohydr. Polym. 157 (2017) 105-113 https://doi.org/10.1016/j.carbpol.2016.09.068.

[6] G. Horvat, T. Fajfar, A. Perva Uzunalić, Ž. Knez, Z. Novak, Thermal properties of polysaccharide aerogels, J. Therm. Anal. Calorim. 127(1) (2016) 363-370 https://doi.org/10.1007/s10973-016-5814-y.

[7] H. Maleki, S. Montes, N. Hayati-Roodbari, F. Putz, N. Huesing, Compressible, Thermally Insulating, and Fire Retardant Aerogels through Self-Assembling Silk Fibroin Biopolymers Inside a Silica Structure- An Approach towards 3D Printing of Aerogels, ACS Appl. Mater. Interfaces 10(26) (2018) 22718–22730 DOI: 10.1021/acsami.8b05856.

[8] Y. Kobayashi, T. Saito, A. Isogai, Aerogels with 3D Ordered Nanofiber Skeletons of Liquid-Crystalline Nanocellulose Derivatives as Tough and Transparent Insulators, Angew. Chem. Int. Ed. 53(39) (2014) 10394-10397 DOI: 10.1002/anie.201405123.

[9] C. Rudaz, R. Courson, L. Bonnet, S. Calas-Etienne, H. Sallée, T. Budtova, Aeropectin: Fully Biomass-Based Mechanically Strong and Thermal Superinsulating Aerogel, Biomacromolecules 15(6) (2014) 2188-2195 DOI: 10.1021/bm500345u.

[10] S. Takeshita, S. Yoda, Chitosan Aerogels: Transparent, Flexible Thermal Insulators, Chem. Mater. 27(22) (2015) 7569-7572 DOI: 10.1021/acs.chemmater.5b03610.

[11] S. Takeshita, S. Yoda, Translucent, hydrophobic, and mechanically tough aerogels constructed from trimethylsilylated chitosan nanofibers, Nanoscale 9(34) (2017) 12311-12315 DOI: 10.1039/C7NR04051B.

[12] S.F. Plappert, J.-M. Nedelec, H. Rennhofer, H.C. Lichtenegger, F.W. Liebner, Strain Hardening and Pore Size Harmonization by Uniaxial Densification: A Facile Approach toward Superinsulating Aerogels from Nematic Nanofibrillated 2,3-Dicarboxyl Cellulose, Chem. Mater. 29(16) (2017) 6630-6641 DOI: 10.1021/acs.chemmater.7b00787.

[13] F. Fischer, A. Rigacci, R. Pirard, S. Berthon-Fabry, P. Achard, Cellulose-based aerogels, Polymer 47(22) (2006) 7636-7645 http://dx.doi.org/10.1016/j.polymer.2006.09.004.

[14] M. Schestakow, I. Karadagli, L. Ratke, Cellulose aerogels prepared from an aqueous zinc chloride salt hydrate melt, Carbohydr. Polym. 137 (2016) 642-649 https://doi.org/10.1016/j.carbpol.2015.10.097.

[15] C.A. García-González, M. Alnaief, I. Smirnova, Polysaccharide-based aerogels—Promising biodegradable carriers for drug delivery systems, Carbohydr. Polym. 86(4) (2011) 1425-1438 http://dx.doi.org/10.1016/j.carbpol.2011.06.066.

[16] M. Alnaief, R. Obaidat, H. Mashaqbeh, Effect of processing parameters on preparation of carrageenan aerogel microparticles, Carbohydr. Polym. 180 (2018) 264-275 https://doi.org/10.1016/j.carbpol.2017.10.038.

[17] I. Smirnova, P. Gurikov, Aerogel production: Current status, research directions, and future opportunities, J. Supercrit. Fluids 134 (2018) 228-233 https://doi.org/10.1016/j.supflu.2017.12.037.

[18] F. Deuber, S. Mousavi, L. Federer, C. Adlhart, Amphiphilic Nanofiber-Based Aerogels for Selective Liquid Absorption from Electrospun Biopolymers, Adv. Mater. Interfaces 4(12) (2017) 1700065 DOI: 10.1002/admi.201700065.

[19] F. Deuber, S. Mousavi, M. Hofer, C. Adlhart, Tailoring pore structure of ultralight electrospun sponges by solid templating, ChemistrySelect 1(18) (2016) 5595-5598 https://doi.org/10.1002/slct.201601084.

[20] F. Deuber, S. Mousavi, L. Federer, M. Hofer, C. Adlhart, Exploration of Ultralight Nanofiber Aerogels as Particle Filters: Capacity and Efficiency, ACS Appl. Mater. Interfaces 10(10) (2018) 9069-9076 DOI: 10.1021/acsami.8b00455.

[21] S. Mousavi, F. Deuber, S. Petrozzi, L. Federer, M. Aliabadi, F. Shahraki, C. Adlhart, Efficient dye adsorption by highly porous nanofiber aerogels, Colloids Surf., A 547 (2018) 117-125 https://doi.org/10.1016/j.colsurfa.2018.03.052.

[22] R.G. Martinez, E. Goiti, G. Reichenauer, S. Zhao, M. Koebel, A. Barrio, Thermal assessment of ambient pressure dried silica aerogel composite boards at laboratory and field scale, Energy and Buildings 128 (2016) 111-118 https://doi.org/10.1016/j.enbuild.2016.06.071.

[23] C. Stepanian, Highly flexible aerogel insulated textile-like blankets, US Patents, US20070154698A1, 2007.

[24] T. Zhou, X. Cheng, Y. Pan, C. Li, L. Gong, H. Zhang, Mechanical performance and thermal stability of glass fiber reinforced silica aerogel composites based on co-precursor method by freeze drying, Appl. Surf. Sci. 437 (2018) 321-328 https://doi.org/10.1016/j.apsusc.2017.12.146.

[25] S. Salomo, T.X. Nguyen, D.K. Le, X. Zhang, N. Phan-Thien, H.M. Duong, Advanced Fabrication and Properties of Hybrid Polyethylene Tetraphalate Fiber-Silica Aerogels from Plastic Bottle Waste, Colloids Surf., A (2018) https://doi.org/10.1016/j.colsurfa.2018.08.015.

[26] J.C.H. Wong, H. Kaymak, P. Tingaut, S. Brunner, M.M. Koebel, Mechanical and thermal properties of nanofibrillated cellulose reinforced silica aerogel composites, Microporous Mesoporous Mater. 217 (2015) 150-158 https://doi.org/10.1016/j.micromeso.2015.06.025.

[27] J. Fu, S. Wang, C. He, Z. Lu, J. Huang, Z. Chen, Facilitated fabrication of high strength silica aerogels using cellulose nanofibrils as scaffold, Carbohydr. Polym. 147 (2016) 89-96 http://dx.doi.org/10.1016/j.carbpol.2016.03.048.

[28] H.-Y. Mi, X. Jing, H.-X. Huang, X.-F. Peng, L.-S. Turng, Superhydrophobic Graphene/Cellulose/Silica Aerogel with Hierarchical Structure as Superabsorbers for High Efficiency Selective Oil Absorption and Recovery, Ind. Eng. Chem. Res. 57(5) (2018) 1745-1755 DOI: 10.1021/acs.iecr.7b04388.

[29] E. Kelechi, O.A. Elvis, A.K. Kanayo, Synthesis and Characterization of Chitosan–Silica Hybrid Aerogel using Sol-Gel Method, Journal of King Saud University-Science (2018) https://doi.org/10.1016/j.jksus.2018.08.005.

[30] M.C. Rodríguez-Robledo, M.A. González-Lozano, P. Ponce-Peña, P. Quintana Owen, M.A. Aguilar-González, G. Nieto-Castañeda, E. Bazán-Mora, R. López-Martínez, G. Ramírez-Galicia, M. Poisot, Cellulose-Silica Nanocomposites of High Reinforcing Content with Fungi Decay Resistance by One-Pot Synthesis, Materials 11(4) (2018) 575 DOI:10.3390/ma11040575.

[31] L. Vasquez-Zacarias, P. Ponce-Peña, T. Pérez-López, E.A. Franco-Urquiza, G. Ramirez-Galicia, M. Poisot, Hybrid Cellulose–Silica Materials from Renewable Secondary Raw Resources: An Eco-friendly Method, Global Challenges (2018) 1700119 https://doi.org/10.1002/gch2.201700119.

[32] N. Rangelova, L. Aleksandrov, S. Nenkova, Synthesis and characterization of pectin/SiO 2 hybrid materials, J. Sol-Gel Sci. Technol. 85(2) (2018) 330-339 https://doi.org/10.1007/s10971-017-4556-z.

[33] C. Wang, H. Cheng, C. Hong, X. Zhang, T. Zeng, Lightweight chopped carbon fibre reinforced silica-phenolic resin aerogel nanocomposite: facile preparation, properties and application to

thermal protection, Composites Part A: Applied Science and Manufacturing (2018) https://doi.org/10.1016/j.compositesa.2018.05.026.

[34] Y.-G. Kim, H.S. Kim, S.M. Jo, S.Y. Kim, B. Yang, J. Cho, S. Lee, J.E. Cha, Thermally insulating, fire-retardant, smokeless and flexible polyvinylidene fluoride nanofibers filled with silica aerogels, Chem. Eng. J. (2018) https://doi.org/10.1016/j.cej.2018.06.102.

[35] S. Zhao, Z. Zhang, G. Sèbe, R. Wu, R.V. Rivera Virtudazo, P. Tingaut, M.M. Koebel, Multiscale Assembly of Superinsulating Silica Aerogels Within Silylated Nanocellulosic Scaffolds: Improved Mechanical Properties Promoted by Nanoscale Chemical Compatibilization, Adv. Funct. Mater. 25(15) (2015) 2326-2334 DOI: 10.1002/adfm.201404368.

[36] G. Hayase, K. Kanamori, K. Abe, H. Yano, A. Maeno, H. Kaji, K. Nakanishi, Polymethylsilsesquioxane–Cellulose Nanofiber Biocomposite Aerogels with High Thermal Insulation, Bendability, and Superhydrophobicity, ACS Appl. Mater. Interfaces 6(12) (2014) 9466-9471 DOI: 10.1021/am501822y.

[37] H. Sai, R. Fu, J. Xiang, Y. Guan, F. Zhang, Fabrication of elastic silica-bacterial cellulose composite aerogels with nanoscale interpenetrating network by ultrafast evaporative drying, Compos. Sci. Technol. 155 (2018) 72-80 https://doi.org/10.1016/j.compscitech.2017.11.004.

[38] J.P. Randall, M.A.B. Meador, S.C. Jana, Polymer reinforced silica aerogels: effects of dimethyldiethoxysilane and bis(trimethoxysilylpropyl)amine as silane precursors, J. Mater. Chem. A 1(22) (2013) 6642-6652 DOI: 10.1039/C3TA11019B.

[39] M.A.B. Meador, E.F. Fabrizio, F. Ilhan, A. Dass, G. Zhang, P. Vassilaras, J.C. Johnston, N. Leventis, Cross-linking amine-modified silica aerogels with epoxies: mechanically strong lightweight porous materials, Chem. Mater. 17(5) (2005) 1085-1098 DOI: 10.1021/cm048063u.

[40] N. Leventis, A. Palczer, L. McCorkle, G. Zhang, C. Sotiriou-Leventis, Nanoengineered silica-polymer composite aerogels with no need for supercritical fluid drying, J. Sol-Gel Sci. Technol. 35(2) (2005) 99-105 https://doi.org/10.1007/s10971-005-1372-7.

[41] S. Iswar, G.M. Snellings, S. Zhao, R. Erni, Y.K. Bahk, J. Wang, M. Lattuada, M.M. Koebel, W.J. Malfait, Reinforced and superinsulating silica aerogel through in situ cross-linking with silane terminated prepolymers, Acta Mater. 147 (2018) 322-328 https://doi.org/10.1016/j.actamat.2018.01.031.

[42] S. Zhao, W.J. Malfait, A. Demilecamps, Y. Zhang, S. Brunner, L. Huber, P. Tingaut, A. Rigacci, T. Budtova, M.M. Koebel, Strong, Thermally Superinsulating Biopolymer–Silica Aerogel Hybrids by Cogelation of Silicic Acid with Pectin, Angew. Chem. Int. Ed. 54(48) (2015) 14282-14286 DOI: 10.1002/anie.201507328.

[43] S. Zhao, W.J. Malfait, E. Jeong, B. Fischer, Y. Zhang, H. Xu, E. Angelica, W.M. Risen, J.W. Suggs, M.M. Koebel, Facile One-Pot Synthesis of Mechanically Robust Biopolymer–Silica Nanocomposite Aerogel by Cogelation of Silicic Acid with Chitosan in Aqueous Media, ACS Sustainable Chem. Eng. 4(10) (2016) 5674-5683 DOI: 10.1021/acssuschemeng.6b01574.

[44] Z. Fei, Z. Yang, G. Chen, K. Li, Preparation of tetraethoxysilane-based silica aerogels with polyimide cross-linking from 3, 3′, 4, 4′-biphenyltetracarboxylic dianhydride and 4, 4′-oxydianiline, J. Sol-Gel Sci. Technol. 85(3) (2018) 506-513 https://doi.org/10.1007/s10971-017-4566-x.

[45] H. Li, C. Sun, R. Li, Y. Fu, L. Song, A. Yang, H. Liu, Preparation and characterization of silica aerogel/polymethyl methacrylate composites with electrostatic interaction phase interface, J. Polym. Eng. 38(8) (2018) 811-818 https://doi.org/10.1515/polyeng-2017-0402.

[46] V.G. Parale, K.-Y. Lee, H.-Y. Nah, H. Choi, T.-H. Kim, V.D. Phadtare, H.-H. Park, Facile synthesis of hydrophobic, thermally stable, and insulative organically modified silica aerogels using co-precursor method, Ceram. Int. 44(4) (2018) 3966-3972 https://doi.org/10.1016/j.ceramint.2017.11.189.

[47] G. Zu, T. Shimizu, K. Kanamori, Y. Zhu, A. Maeno, H. Kaji, J. Shen, K. Nakanishi, Transparent, Superflexible Doubly Cross-linked Polyvinylpolymethylsiloxane Aerogel Superinsulators via Ambient Pressure Drying, ACS NANO 12(1) (2018) 521-532 DOI: 10.1021/acsnano.7b07117.

[48] T. Shimizu, K. Kanamori, A. Maeno, H. Kaji, C.M. Doherty, K. Nakanishi, Transparent Ethenylene-Bridged Polymethylsiloxane Aerogels: Mechanical Flexibility and Strength and Availability for Addition Reaction, Langmuir 33(18) (2017) 4543-4550 DOI: 10.1021/acs.langmuir.7b00434.

[49] G. Reichenauer, Structural Characterization of Aerogels, in: M.A. Aegerter, N. Leventis, M.M. Koebel (Eds.), Aerogels Handbook, Springer New York2011, pp. 449-498.

[50] J.C.H. Wong, H. Kaymak, S. Brunner, M.M. Koebel, Mechanical properties of monolithic silica aerogels made from polyethoxydisiloxanes, Microporous Mesoporous Mater. 183 (2014) 23-29 http://dx.doi.org/10.1016/j.micromeso.2013.08.029.

[51] T. Stahl, S. Brunner, M. Zimmermann, K. Ghazi Wakili, Thermo-hygric properties of a newly developed aerogel based insulation rendering for both exterior and interior applications, Energy and Buildings 44(0) (2012) 114-117 http://dx.doi.org/10.1016/j.enbuild.2011.09.041.

[52] European Standard EN 12667, Thermal performance of building materials and products – determination of thermal resistance by means of guarded hot plate and heat flow meter methods – products of high and medium thermal resistance, Brussels, 2001.

[53] R.S. Singh, G.K. Saini, J.F. Kennedy, Downstream processing and characterization of pullulan from a novel colour variant strain of Aureobasidium pullulans FB-1, Carbohydr. Polym. 78(1) (2009) 89-94 https://doi.org/10.1016/j.carbpol.2009.03.040.

[54] K. Katsuraya, K. Hatanaka, K. Matsuzaki, S. Amiya, Assignment of finely resolved 13C NMR spectra of poly (vinyl alcohol), Polymer 42(24) (2001) 9855-9858 https://doi.org/10.1016/S0032-3861(01)00536-5.

[55] R.D. Huang, M.S. Feather, Carbon-13 NMR study of some Maillard reaction products arising from D-glucose-DL-alanine interactions, J. Agric. Food. Chem. 36(4) (1988) 673-676 DOI: 10.1021/jf00082a001.

[56] W.J. Malfait, R. Verel, M.M. Koebel, Hydrophobization of Silica Aerogels: Insights from Quantitative Solid-State NMR Spectroscopy, J. Phys. Chem. C 118(44) (2014) 25545-25554 DOI: 10.1021/jp5082643.

[57] W.J. Malfait, S. Zhao, R. Verel, S. Iswar, D. Rentsch, R. Fener, Y. Zhang, B. Milow, M.M. Koebel, Surface Chemistry of Hydrophobic Silica Aerogels, Chem. Mater. 27(19) (2015) 6737-6745 DOI: 10.1021/acs.chemmater.5b02801.

[58] N. Hüsing, U. Schubert, Aerogels—Airy Materials: Chemistry, Structure, and Properties, Angew. Chem. Int. Ed. 37 (1998) 22-45 DOI: 10.1002/(sici)1521-3773(19980202)37:1/2<22::aid-anie22>3.0.co;2-i.

[59] J. Kim, T.-H. Song, Vacuum insulation properties of glass wool and opacified fumed silica under variable pressing load and vacuum level, Int. J. Heat Mass Transfer 64 (2013) 783-791 https://doi.org/10.1016/j.ijheatmasstransfer.2013.05.012.

[60] Z. Chen, Z. Chen, Z. Yang, J. Hu, Y. Yang, L. Chang, L.J. Lee, T. Xu, Preparation and characterization of vacuum insulation panels with super-stratified glass fiber core material, Energy 93 (2015) 945-954 https://doi.org/10.1016/j.energy.2015.08.105.

[61] J. Cai, S. Liu, J. Feng, S. Kimura, M. Wada, S. Kuga, L. Zhang, Cellulose–Silica Nanocomposite Aerogels by In Situ Formation of Silica in Cellulose Gel, Angew. Chem. Int. Ed. 51(9) (2012) 2076-2079 DOI: 10.1002/anie.201105730.

[62] G. Markevicius, R. Ladj, P. Niemeyer, T. Budtova, A. Rigacci, Ambient-dried thermal superinsulating monolithic silica-based aerogels with short cellulosic fibers, J. Mater. Sci. 52(4) (2017) 2210-2221 https://doi.org/10.1007/s10853-016-0514-3.

[63] A. Demilecamps, C. Beauger, C. Hildenbrand, A. Rigacci, T. Budtova, Cellulose–silica aerogels, Carbohydr. Polym. 122(0) (2015) 293-300 http://dx.doi.org/10.1016/j.carbpol.2015.01.022.

[64] M.A.B. Meador, L.A. Capadona, Process for preparing polymer reinforced silica aerogels, US Patents, 2011.

[65] M.A.B. Meador, L.A. Capadona, L. McCorkle, D.S. Papadopoulos, N. Leventis, Structure−Property Relationships in Porous 3D Nanostructures as a Function of Preparation Conditions: Isocyanate Cross-Linked Silica Aerogels, Chem. Mater. 19(9) (2007) 2247-2260 DOI: 10.1021/cm070102p.

[66] Z. Zhang, G. Sèbe, D. Rentsch, T. Zimmermann, P. Tingaut, Ultralightweight and Flexible Silylated Nanocellulose Sponges for the Selective Removal of Oil from Water, Chem. Mater. 26(8) (2014) 2659-2668 DOI: 10.1021/cm5004164.

S. Zhao, W. Malfait, C. Adlhart and M. Koebel conceived of the presented idea. A. Wohlhauser synthesized the pullulan/PVA nanofibers. O. Emery and S. Zhao fabricated the composites. W. Malfait assisted with NMR measurements, and S. Zhao did all the rest characterization. W. Malfait wrote the manuscript with support from S. Zhao. M. Koebel helped to supervise the project. All authors provided critical feedback and helped shape the research, analysis and manuscript.